Available online at www.sciencedirect.com
ScienceDirect
Control Engineering Practice 16 (2008) 697–709
CONTROL ENGINEERING PRACTICE
www.elsevier.com/locate/conengprac

Force computation and continuous path tracking for hydraulic parallel manipulators

Jih-Hua Chin[a,*], Yen-His Sun[a], Yuan-Ming Cheng[b]

[a]Department of Mechanical Engineering, National Chiao-Tung University, Hsinchu, 300, Taiwan, ROC
[b]Department of Mechanical and Automation Engineering, Kao Yuan University, Kaohsiung County, 821, Taiwan, ROC

Received 16 May 2006; accepted 10 August 2007
Available online 24 October 2007

Abstract

Machine tools, robots and parallel manipulators are useful platforms in manufacturing. For parallel manipulators, developing contour tracking ability and clarifying the role of force computation are of significance.

This work presents a novel contour tracking control with force computation for hydraulic parallel manipulators. Different trajectories are used to evaluate the tracking errors on an empirical hydraulic parallel manipulator. The proposed control law and tracking systems are effective and the force computation is proven highly effective in the frame of the contour tracking system.

Keywords: Hydraulic manipulator; Parallel manipulator; Contour tracking; Computed force control; Cross-coupled tracking; Pre-compensation tracking

1. Introduction

Ancient humans used tools, whereas modern humans use machine as tools. Machines designed as manufacturing tools are called machine tools. Machine tools are in serial but orthogonal structures. The development of robots has created a new family of machine tools that are serial and non-orthogonal structures. Another machine is emerging and approaching maturity—parallel structured machines that have parallel and non-orthogonal structures.

Parallel manipulators with physically closed forms generally have advantages of high stiffness, low inertia, large loading capacity and compact construction. Parallel manipulators have been widely utilized in numerous applications, such as isolation platforms, endoscopes, vehicle simulators, aircraft simulators, spherical radio telescopes, and six-axis machine tools. Since parallel manipulators have high degrees of freedom and are compact, they are very suited to use as heavy-duty platforms. Hydraulically driven parallel manipulators are such heavy-duty platforms.

The controls of machine tools, robots and parallel manipulators have distinct features. Machine tools are capable of tracking continuous paths; however, no force computation exists for the creation of feeding motion. Robots have limited ability to tracking continuous paths, but computed-torque is the standard control in motion creation—this is true for even the oddest form of serial robots (Khalil, Gallot, & Boyer, 2005). Parallel manipulators have little continuous path tracking ability; however, since parallel manipulators are akin to robots, the torque/force computation is normally executed.

While machine tools and robots have matured in manufacturing, parallel manipulators are still progressing (Merlet, Perng, & Daney, 2000)—the ability of parallel manipulators to perform continuous path tracking is not yet mature.

Generally, hydraulic machines have high load capacity, but poor dynamic characteristics and are thus unable to track trajectories accurately. Numerous studies have been devoted to improve the accuracy and control performance of hydraulic systems. Although concepts for computed force on hydraulic cylinders were proposed by Lischinsky, Canudas-de-Wit, and Morel (1999), they did not consider dynamics. Kwon and Babcock (1995), who compensated

*Corresponding author. Fax: +886 3 5727485.
E-mail address: jhchin@mail.nctu.edu.tw (J.-H. Chin).

0967-0661/$ - see front matter © 2007 Elsevier Ltd. All rights reserved.
doi:10.1016/j.conengprac.2007.08.007

for the load and friction effect in tracking control, did not consider a parallel manipulator and system dynamics. Zhou (1995), who developed a force-compensation controller for hydraulic robots, did not consider parallel manipulators. Kosuge et al. (1996) used feedback force compensation to achieve velocity control, but did not address continuous path tracking.

On the other hand, for orthogonal machine tools, tracking continuous spatial trajectories has been successful. Cross-coupled pre-compensation algorithms (CCPM) (Chin, Cheng, & Lin, 2004; Chin & Lin, 1997, 1999) have been developed. However, no tracking-related algorithms for machine tools compute force. Non-orthogonal parallel manipulators have simple constructions and are sophisticated in kinematics and computations of dynamics (Gosselin & Angeles, 1989; Gosselin & Angeles, 1990; Merlet, 1992); this, combined with the problem of singularity in work space (St-Onge & Gosselin, 2000), generates increasing obstacles for developing comparable continuous contour tracking ability. Lue, Cheng, and Chin (2005) investigated the problem of contour tracking for non-orthogonal machines, but did not utilize experimental implementation. Although there is no lack of powerful control algorithms for manipulators (Benallegue, 1995; Gang, 1990; Honegger, 1997; Rolf, 1990; Walker& Wee, 1991), continuous contour tracking control is still lacking for parallel manipulators (Dasgupta & Mruthyunjaya, 2000). This shortcoming is especially true for heavy-duty hydraulic parallel manipulators.

Parallel manipulators have been the focus of considerable research (Merlet, 2000; www.parallemic.org). This work investigates a relatively weak and insufficiently investigated area—continuous path tracking of hydraulic parallel manipulators. A novel control strategy that compensates for contours and has a force computation combined with velocity control is proposed. The force computation is effective, if not indispensable, for heavy-duty hydraulic manipulators, and the combination of force computation and contour control allows the parallel manipulators to continuously track contours.

2. Kinematics and dynamics of hydraulic manipulator

The empirical 3-DOF hydraulic parallel machine is composed of a moving platform supported on a stationary base by three hydraulic cylinders each having universal joints on both ends, as shown in Fig. 1. Inverse kinematics determines the extension lengths of hydraulic cylinders to create the desired position and orientation of the moving platform. The purpose of continuous contour tracking is to control the three cylinders to track not desired discrete positions and orientations, but desired continuous positional and orientation trajectories. For heavy duty manipulators, force computation is presumably important, so dynamic model is established and inverse dynamics is utilized to derive demand forces for cylinders during the trajectory tracking. Kinematics of this type of manipulators has been investigated in Tsai (1996) and Tsai and Joshi (2003). Dynamic formulations can be established by different mathematical methods, for example, Lagrange (Geng, Haynes, Lee, & Carroll, 1992), principal virtual work method (Tsai, 1999, 2000), etc. In this work Newton-Euler formulation (Dasgupta & Mruthyunjaya, 1998a, b; Harib & Srinivasan, 2003) is used to derive dynamics. And the dynamics of hydraulic will be integrated with dynamics of manipulator.

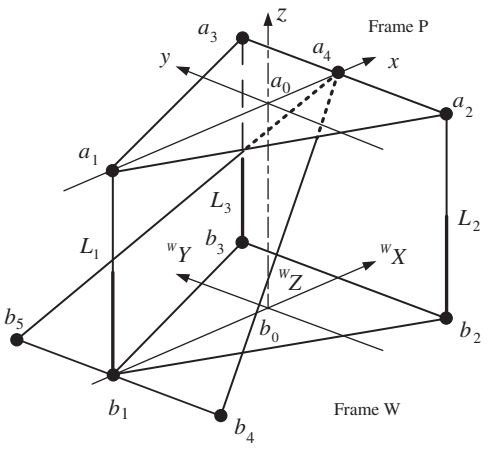

Fig. 1. Construction of hydraulic manipulator.

2.1. Coordinate system

The moving platform of the empirical hydraulic manipulator (Fig. 1) has three DOF and the position and orientation can be represented by a vector $\boldsymbol{q}$ with position and orientation variables (Cheng, 2004)

$$\boldsymbol{q} = (z, \alpha, \beta)^{\mathrm{T}}, \tag{1}$$

where z is Cartesian vector in Z-axis, and α, β are Euler angles. The link space consists of three-variables

$$\boldsymbol{l} = [\, l_1 \quad l_2 \quad l_3 \,]^T. \tag{2}$$

A passive triangular support which may strengthen the structural weakness but do not hinder the necessary motion within work space is connected to the center of platform with a pair of revolute joints. Three robust hydraulic cylinders serve as the driving links.

In Fig. 1 the origin of coordinates $\boldsymbol{P}$ and $\boldsymbol{W}$ is assumed to be on the mass center of moving platform and base, respectively. At initial position, the relation between frame $\boldsymbol{P}$ and frame $\boldsymbol{W}$ is as follows:

$$^W\boldsymbol{P} = \begin{pmatrix} 0 & 0 & z \end{pmatrix}^T \tag{3}$$

After rotational transformation the relation can be written as (Dasgupta & Mruthyunjaya, 1998a)

$$^W\boldsymbol{P} = (\, 0 \quad 0 \quad z_P \,)^{\mathrm{T}} + {}^W R_P {}^P\boldsymbol{P}. \tag{4}$$

Fig. 2 illustrates the top view of the hydraulic manipulator. The connecting points on upper platform

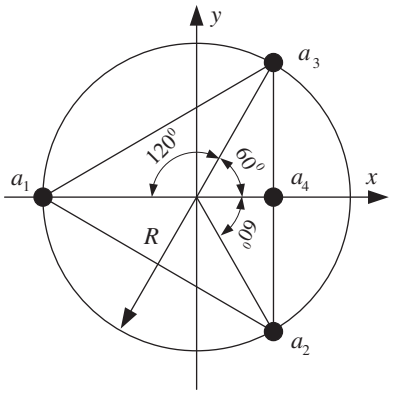

Fig. 2. Top view of the hydraulic manipulator.

are in moving coordinates:

$$^{P}\boldsymbol{a}_i = [\,R\cdot c\theta_i \quad R\cdot s\theta_i \quad 0], \quad i = 1{-}3$$

and those on the lower platform are in fixed coordinates:

$$^{W}\boldsymbol{b}_i = [\,R\cdot c\theta_i \quad R\cdot s\theta_i \quad 0], \quad \theta_i = \pi + \frac{2\pi}{3}(i-1), \quad i = 1{-}3,$$

where $\boldsymbol{c}$ and $\boldsymbol{s}$ denote *cosine* and *sine* function, respectively.

The connecting points of the upper platform described in fixed coordinates are

$$^{W}\boldsymbol{a}_i = [^{W}R_P]*[^{P}\boldsymbol{a}_i], \quad i = 1{-}3,$$

where $^{W}R_P$ is the rotational matrix, and

$$^{W}R_P = R(y,\beta)R(x,\alpha) = \begin{bmatrix} c\beta & s\beta s\alpha & s\beta c\alpha \\ 0 & c\alpha & -s\alpha \\ -s\beta & c\beta s\alpha & c\beta c\alpha \end{bmatrix}. \tag{5}$$

2.2. Inverse kinematics

2.2.1. Inverse position kinematics

In Fig. 1, the points $\boldsymbol{a}_i$ ($i = 1,2,3$) on the moving platform are joint locations which can be referenced to frame $\boldsymbol{W}$ from frame $\boldsymbol{P}$ as (Dasgupta & Mruthyunjaya, 1998a)

$$^{W}\boldsymbol{a}_i = {}^{W}\boldsymbol{x}_p + {}^{W}R_P{}^{P}\boldsymbol{a}_i, \quad {}^{W}x_p = [0,0,z]^{\mathrm{T}} \tag{6}$$

and the link vector $\boldsymbol{L}_i$ can be expressed as

$$^{W}\boldsymbol{L}_i = {}^{W}\boldsymbol{a}_i - {}^{W}\boldsymbol{b}_i, \tag{7}$$

where b_i are joint vectors with respect to center of frame W, namely the center of fixed platform.

2.2.2. Inverse velocity kinematics

The velocity of $\boldsymbol{a}_i$ is determined by taking time differentiation of Eq. (6):

$$^{W}\dot{\boldsymbol{a}}_i = {}^{W}\dot{\boldsymbol{x}}_p + \boldsymbol{\omega_P} \times {}^{W}R_P{}^{\boldsymbol{P}}\boldsymbol{a}_i, \quad {}^{W}\dot{\boldsymbol{x}}_p = [0,0,\dot{z}]^{\mathrm{T}}$$

and

$$\boldsymbol{\omega_P} = [\,\dot{\alpha} \quad \dot{\beta} \quad 0\,]^{\mathrm{T}}. \tag{8}$$

Then, the link velocity is projection of velocity vector $\boldsymbol{a}_i$ on the link vector $\boldsymbol{n}_i$

$$\dot{l}_i = {}^{W}\dot{\boldsymbol{a}}_i \cdot {}^{W}\boldsymbol{n}_i = {}^{W}\dot{\boldsymbol{x}}_p \cdot {}^{W}\boldsymbol{n}_i + \boldsymbol{\omega_P} \cdot \left({}^{W}R_P{}^{P}\boldsymbol{a}_i \times {}^{W}\boldsymbol{n}_i\right). \tag{9}$$

The singular position will occur when $\det(\boldsymbol{J}) = 0$, but in the work space of the exemplary manipulator there is no singular surface.

2.2.3. Inverse acceleration kinematics

The acceleration of $\boldsymbol{a}_i$ is determined by differentiating Eq. (8) (Dasgupta & Mruthyunjaya, 1998a)

$$^{\boldsymbol{W}}\ddot{\boldsymbol{a}}_i = {}^{\boldsymbol{W}}\ddot{\boldsymbol{x}}_p + \boldsymbol{\alpha_P} \times {}^{W}R_P{}^{\boldsymbol{P}}\boldsymbol{a}_i + \boldsymbol{\omega}_p \times \left(\boldsymbol{\omega_P} \times {}^{W}R_P{}^{\boldsymbol{P}}\boldsymbol{a}_i\right),$$
$$^{W}\ddot{\boldsymbol{x}}_p = [0,0,\ddot{z}]^{\mathrm{T}}. \tag{10}$$

Therefore, the $\ddot{l}_i$ can be easily found by differentiating Eq. (9) with respect to time

$$\ddot{l}_i = {}^{W}\ddot{\boldsymbol{a}}_i \cdot {}^{W}\boldsymbol{n}_i - l_i\left(\boldsymbol{\omega}_i \times \left(\boldsymbol{\omega}_i \times {}^{W}\dot{\boldsymbol{n}}_i\right)\right) \cdot {}^{W}\boldsymbol{n}_i, \tag{11}$$

where the limb angular velocity $\boldsymbol{\omega_i}$ and angular acceleration $\boldsymbol{\alpha_i}$ are as follows

$$\boldsymbol{\omega_i} = \left({}^{W}\boldsymbol{n}_i \times {}^{W}\dot{\boldsymbol{a}}_i\right)/l_i, \quad \boldsymbol{\alpha_i} = \left({}^{W}\boldsymbol{n}_i \times {}^{W}\ddot{\boldsymbol{a}}_i - 2\dot{l}_i\boldsymbol{\omega_i}\right)/l_i. \tag{12}$$

2.3. Inverse dynamics

Dynamic equations can be derived by different approaches: Newton–Euler formulation, Lagrangian formulation, and the principle of virtual work method. In this paper, Newton–Euler formulation is used (Dasgupta & Mruthyunjaya, 1998b) (Fig. 3).

Let m_p and I_p be mass and inertia moment of platform, the force f_i of link i, $i = 1, 2, 3$, is determined by summing reaction forces along axial direction and expressed as (Dasgupta & Mruthyunjaya, 1998b)

$$f_i = m_u\boldsymbol{a_{iu}} \cdot {}^{W}\boldsymbol{n_i} - f_i^a - m_u\boldsymbol{G} \cdot {}^{W}\boldsymbol{n_i}. \tag{13}$$

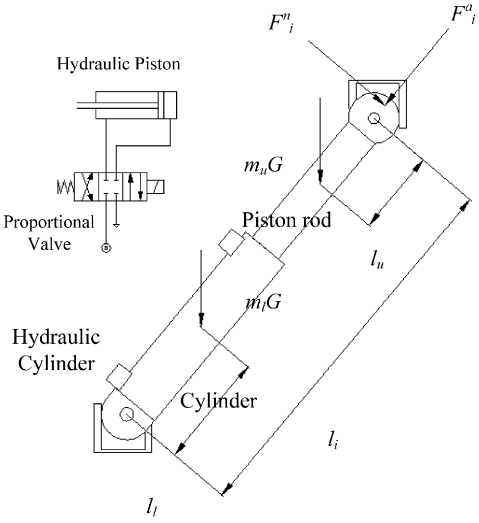

Fig. 3. Force components and length expressions on link i.

The actuation force of links $\boldsymbol{F}$ can be derived as

$$\boldsymbol{F} = \begin{pmatrix} f_1 \\ \vdots \\ f_3 \end{pmatrix} = \begin{pmatrix} m_u(\boldsymbol{a}_{1u} - \boldsymbol{G}) \cdot \boldsymbol{n}_1 \\ \vdots \\ m_u(\boldsymbol{a}_{3u} - \boldsymbol{G}) \cdot \boldsymbol{n}_3 \end{pmatrix} - J^{\mathrm{T}} C, \tag{14}$$

where

$$C = \begin{bmatrix} \left(m_p {}^W\ddot{\boldsymbol{x}}_{\boldsymbol{P}} - m_p \boldsymbol{G} - \sum_{i=1}^{3} \boldsymbol{F}_i^n \right)_z \\ \left(-I_P \boldsymbol{\alpha}_{\boldsymbol{P}} + I_P \boldsymbol{\omega}_{\boldsymbol{P}} \times \boldsymbol{\omega}_{\boldsymbol{P}} - \sum_{i=1}^{3} {}^W R_P {}^P a_i \times F_i^n - \sum_{i=1}^{3} \boldsymbol{M}_i \right)_{x,y} \end{bmatrix}, \tag{15}$$

$$J^{-T} = \begin{bmatrix} {}^W\boldsymbol{n}_{1,z} & \cdots & {}^W\boldsymbol{n}_{3,z} \\ \left({}^W R_P {}^P \boldsymbol{a}_1 \times {}^W\boldsymbol{n}_1 \right)_{x,y} & \cdots & \left({}^W R_P {}^P \boldsymbol{a}_3 \times {}^W\boldsymbol{n}_3 \right)_{x,y} \end{bmatrix}. \tag{16}$$

The Jacobians are established in a preceding study (Cheng, 2004)

$$J = \begin{bmatrix} \frac{\partial L_1}{\partial Z} & \frac{\partial L_1}{\partial \alpha} & \frac{\partial L_1}{\partial \beta} \\ \frac{\partial L_2}{\partial Z} & \frac{\partial L_2}{\partial \alpha} & \frac{\partial L_2}{\partial \beta} \\ \frac{\partial L_3}{\partial Z} & \frac{\partial L_3}{\partial \alpha} & \frac{\partial L_3}{\partial \beta} \end{bmatrix} = \begin{bmatrix} J_{11} & J_{12} & J_{13} \\ J_{21} & J_{22} & J_{23} \\ J_{31} & J_{32} & J_{33} \end{bmatrix}.$$

With

$$\begin{aligned} J_{i1} &= ({}^W\boldsymbol{a}_{iz} - {}^W\boldsymbol{b}_{iz})/L_i \\ J_{i2} &= [({}^W\boldsymbol{a}_{ix} - {}^W\boldsymbol{b}_{ix}) \cdot R \cdot s\theta_i \cdot c\alpha \cdot s\beta \\ &\quad + ({}^W\boldsymbol{a}_{iy} - {}^W\boldsymbol{b}_{iy}) \cdot R \cdot s\theta_i \cdot (-s\alpha) + ({}^W\boldsymbol{a}_{iz} - {}^W\boldsymbol{b}_{iz}) \cdot R \cdot s\theta_i \cdot c\alpha \cdot c\beta]/L_i, \\ J_{i3} &= [({}^W\boldsymbol{a}_{ix} - {}^W\boldsymbol{b}_{ix}) \cdot R \cdot (c\theta_i \cdot (-s\beta) + s\theta_i \cdot s\alpha \cdot c\beta) \\ &\quad + ({}^W\boldsymbol{a}_{iz} - {}^W\boldsymbol{b}_{iz}) \cdot R \cdot (c\theta_i \cdot (-c\beta) + s\theta_i \cdot s\alpha \cdot (-s\beta))]/L_i, \end{aligned}$$

where $i = 1$–3.

There are efficient modeling algorithms (Ibrahim, Khalil, & Guegan, 2004; Khalil & Guegan, 2004) which may give efficient close-form solutions to the parallel manipulators, but Eqs. (1)–(14) are used in the force computation and controller design in this study for the sake of consistence with former studies.

2.4. Forward kinematics

Forward kinematics is to find the Cartesian coordinate vector of platform from links information. Solutions are not unique. Raghavan (1993) had solved the forward kinematics with multi-possible solutions, but only one solution is consistent with actual position of platform. A Newton–Raphson method based numerically iterative method for forward kinematics was used by Chin and Peng (2005a) which was followed in this work.

For solving the problem, a closed-loop function $FL_i(q)$ is defined as (Sirouspour & Salcudean, 2001)

$$FL(\boldsymbol{q}) = \sum_{i=1}^{3} \left(L_i(q)^2 - l_i^2 \right) = 0, \tag{17}$$

where $\boldsymbol{i}$ denotes link number and $L_i(q)$ is link length function, which determines the link length by inverse kinematics with coordinate vector $\boldsymbol{q}$.

The desired vector $\boldsymbol{q}_{(n)}$ can be easily computed as (Chin & Peng, 2005a)

$$\boldsymbol{q}_{(n)} = \boldsymbol{q}_{(n-1)} + J \cdot \left(FL(\boldsymbol{q})|_{\boldsymbol{q}=\boldsymbol{q}_{(n)}} - FL(\boldsymbol{q})|_{\boldsymbol{q}=\boldsymbol{q}_{(n-1)}} \right). \tag{18}$$

2.5. Forward dynamics

Forward dynamics equations, which were usually used for simulating motion process of manipulator, derive the position, velocity, and acceleration from information of link force. The manipulator link force can be found by (Sirouspour & Salcudean, 2001)

$$\boldsymbol{F} = M(\boldsymbol{q}_a)\ddot{\boldsymbol{q}} + \boldsymbol{N}(\boldsymbol{q}_a, \dot{\boldsymbol{q}}_a) + \boldsymbol{G}(\boldsymbol{q}_a), \tag{19}$$

where $\boldsymbol{M}$ is inertia mass matrix, $\boldsymbol{N}$ is vector of centrifugal/Coriolis force, and $\boldsymbol{G}$ is vector of gravitational force.

In this work simulation is performed by an algorithm similar to that in Sirouspour and Salcudean (2001). Fig. 4 describes the simulation algorithm.

2.6. Dynamics of hydraulic cylinder

The links of manipulator are hydraulic cylinders. Some control schemes for improving hydraulic tracking were seen in the literature, for instance, PID controller (Liu & Daley, 2000) or the adaptive control of hydraulic cylinder (Siciliano & Villani, 1996). The load force is a factor that influences the performance adversely (Merrit, 1967). Therefore, computed force is indispensable for hydraulic manipulator to cope with the force effect (Fig. 5).

The load flow Q_L supplied by valve is a function of spool displacement x_v and load pressure P_L (Merrit, 1967)

$$Q_L = \frac{(Q_1 + Q_2)}{2} = K_v x_v - K_p P_L, \tag{20}$$

where K_v and K_p are valve coefficients, and $P_L = P_1 - P_2$.

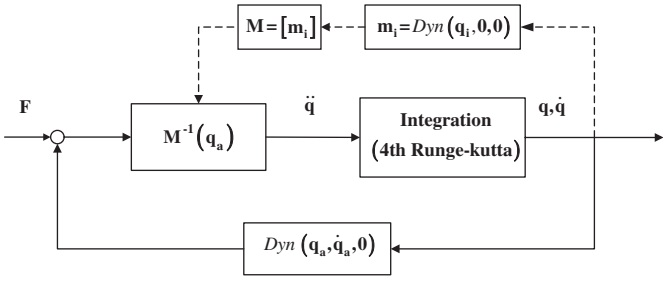

Fig. 4. Simulation block diagram (Sirouspour & Salcudean, 2001).

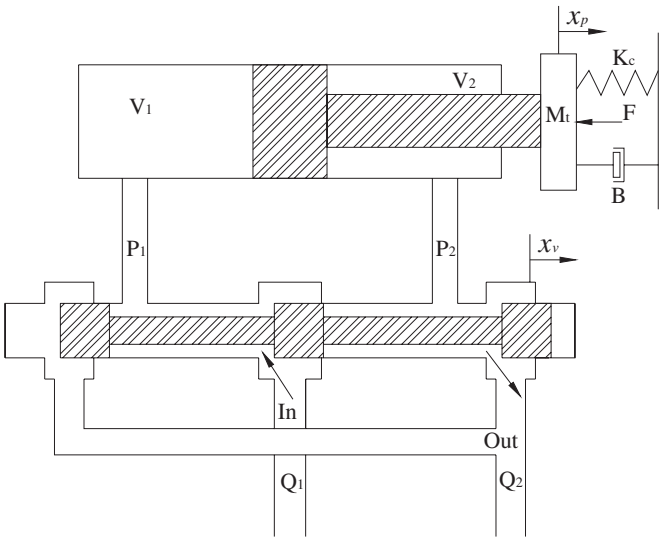

Fig. 5. Servo-valve and cylinder system (Merrit, 1967).

The load flow in cylinder is the load flow supplied by valve, thus

$$Q_L = A_p\dot{x}_p + C_l P_L = K_v x_v - K_p P_L, \tag{21}$$

where x_p is piston displacement, A_p is area of piston, V is total volume of cylinder chamber, and C_l is leakage coefficient. The actuating piston force F_L is approximately $A_p P_L$, so that piston velocity can be obtained from (21) as

$$\dot{x}_p = \frac{K_v}{A_p}x_v - \frac{(C_l + K_p)}{A_p}\frac{F_L}{A_p}. \tag{22}$$

3. Control laws

A force control law is now proposed to form the core for manipulator control. The force control begins with the control of valve spool displacement. Spool displacement is proportional to input voltage u_v and, using Eq. (26), the valve control input can be expressed in terms of $\dot{x}_p$ and F_L

$$u_v = \frac{x_v}{k_{iv}} = \frac{A_p}{k_{iv}K_v}\dot{x}_p + \frac{(C_l + K_p)}{K_v k_{iv}}\frac{F_L}{A_p} = k_1\dot{x}_p + k_2 F_L, \tag{23}$$

where u_v is voltage input of servo-valve, k_{iv} is a constant, and k_1, k_2 are clustered constants.

The F_L is computed (desired) force and a control concept of computed force is introduced here

$$u_v = k_1\dot{x}_p^d + k_2 F_L, \tag{24}$$

where $\dot{x}_p^d$ is modified desired piston velocity created as follows:

$$\dot{x}_p^d = \dot{x}_{p,d} + K_p(x_{p,d} - x_{p,a}). \tag{25}$$

with K_p a proportional gain. The tracking error e is guaranteed to converge to zero when K_p is positive:

$$\dot{e} + K_p e = 0, \quad e = x_{p,d} - x_{p,a}. \tag{26}$$

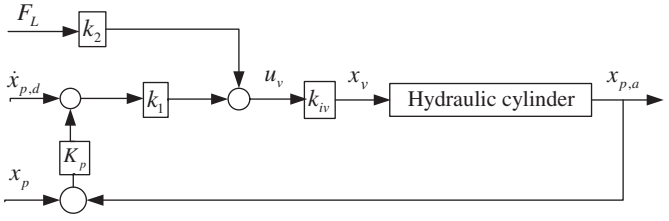

Fig. 6. A control strategy taking care of force and position error.

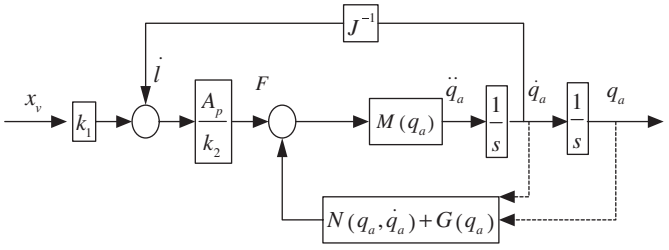

Fig. 7. Computer simulator of hydraulic manipulator with hydraulic actuator.

The control strategy of trajectory tracking with force computation is shown in Fig. 6. The control command to valve is formed by taking into consideration of desired output force F_L, the desired piston velocity $\dot{x}_{p,d}$, and the error between the desired piston position x_p and the actual piston position $x_{p,a}$.

The spirit of the control strategy shown in Fig. 6 is that the load force is computed from inverse dynamics and the position error is compensated.

The command voltage $\boldsymbol{u_v}$ to valve in Fig. 6 is formed by $\boldsymbol{u_1}$ and $\boldsymbol{u_2}$.

$$\boldsymbol{u}_1 = k_2\boldsymbol{F}_L, \quad \boldsymbol{u}_2 = k_1\dot{\boldsymbol{x}}_p^d. \tag{27}$$

Combining with forward dynamic discussed in Section 2.5, computer simulator for hydraulic manipulator with dynamics of hydraulic actuators is shown in Fig. 7.

4. Control systems for contour tracking and force computation

Based on the control laws discussed in the last section, four control systems will be proposed to give the hydraulic manipulator ability of continuous path tracking and force computation.

The basic tracking ability of orthogonal machine tools is the point-by-point position control. For higher order trajectory the contour fidelity is enhanced by contour tracking. Some cross-coupled compensation systems for contour tracking have been proposed (Koren, 1980; Koren & Lo, 1991; Sarachik & Ragazzini, 1957). Speed pre-compensation for machine tools was first proposed by Huan (1982). Chin and Tsai (1993) extended the idea to non-orthogonal robot. Chin and Lin (1997) integrated cross-coupled compensation and speed pre-compensation to form a high speed high curvature tracking system for

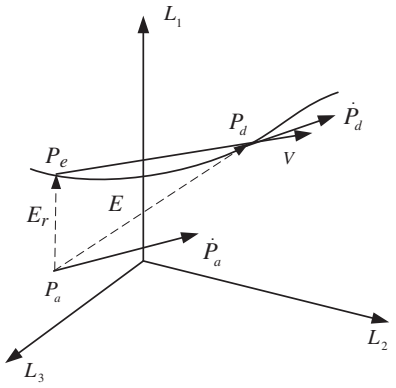

Fig. 8. Spatial path contour error.

machine tools. Further developments included special trajectory algorithm (Chin & Lin, 1999), Fuzzy application (Chin et al., 2004), but only for orthogonal machine tools. Lue et al. (2005) proposed a tracking frame work for non-orthogonal machines, but there were no experimental verification.

For the sake of completeness, the contour error and the contour compensation is first given in the following.

4.1. Contour error

Contour fidelity can be enhanced by diminishing contour error during tracking. Fig. 8 illustrates contour error between desired path and actual position.

In Fig. 8, $\boldsymbol{P}_a$ is the actual position of manipulator, and $\boldsymbol{P}_e$ is the point most close to $\boldsymbol{P}_a$ on the desired path. The vector $\boldsymbol{E}$ is position tracking error vector which is from actual position $\boldsymbol{P}_a$ to desired position $\boldsymbol{P}_d$.

$$\boldsymbol{E} = \boldsymbol{P}_d - \boldsymbol{P}_a = \begin{bmatrix} E_1 & E_2 & E_3 \end{bmatrix}^{\mathrm{T}}, \tag{28}$$

where subscript number means piston's numbering. $\boldsymbol{E}_r$ is the contour error vector which is the shortest distance between desired trajectory and actual position

The contour error $\boldsymbol{E}_r$ is given in (Lue et al., 2005).

4.2. Velocity pre-compensation

Error vector $\boldsymbol{E}_r$ is used to generate the velocity compensation for diminishing contour error. PI controller is designed for modifying velocity. A velocity pre-compensation control is proposed in Cheng and Chin (2003):

$$\vec{\boldsymbol{V}} = \vec{\underset{a}{\boldsymbol{V}}} + K_v \vec{\underset{r}{\boldsymbol{E}}} + K_{iv} \int \vec{\underset{r}{\boldsymbol{E}}}\, \mathrm{d}t. \tag{29}$$

4.3. Four control systems for trajectory tracking and force computation

Based upon the proposed control laws and strategy (Fig. 6), four different control systems were constructed. Fig. 9(a) is the basic velocity control for the hydraulic parallel manipulator. Since the cross-coupled pre-compensation method (CCPM) is a speed-oriented contour tracking control, the velocity control forms a base stone for comparison. Fig. 9(b) is the velocity control with force computation. Fig. 9(c) is the velocity control with cross-coupled pre-compensation and Fig. 9(d) is the ultimate control system, velocity control with CCPM and force computation. System in Fig. 9(d) is a new idea not yet investigated before.

5. Experiments

5.1. Set-up of hydraulic manipulator

The empirical hydraulic manipulator rig is shown in Fig. 10. In order to exclude singularities the manipulator is constrained by an inclined support, which provides vertical restriction. The initial length of hydraulic cylinder is 500 mm and the stroke is 400 mm. The cylinders are controlled by servo-capable proportional valve of brand D1FH (Parker$^{\mathrm{TM}}$). The control voltage range is ± 10 V. Each cylinder is connected to platform and the stationary base by two universal joints on both ends, and oil supply is at constant pressure of 10 bar.

The entire hydraulic manipulator system is shown in Fig. 11. The valve has a band-width of 100 Hz of operation, which allows sampling time of 10 ms. Two ADDA interface cards brand PCI-9111 and ACL-6128 were used. The stroke of cylinder is monitored by potentiometer scale.

5.2. Controller design

Computed force controller is implemented as proposed in Section 3. System block diagram is seen in Fig. 9(b) and 9(d).

Physical constants of hydraulic cylinder are obtained by calibrations. A tiny "dead zone" is seen around the zero point while the load 38.5 kg appears no apparent influence on the linearity of the relationships. The load 38.5 kg is a static load on the upper platform, there is no contact impact. If there is contact impact a stabilizing control should be included (Sekhavat, Sepehri, & Wu, 2006).

The following empirical constants were obtained from calibration:

$$k_1^{cyl1} = 0.0206\left(\frac{\text{voltage}}{\text{mm/sec}}\right), \quad k_1^{cyl2} = 0.0191\left(\frac{\text{voltage}}{\text{mm/sec}}\right),$$

$$fk_1^{cyl3} = 0.0202\left(\frac{\text{voltage}}{\text{mm/sec}}\right).$$

Constant k_2 is obtained from Eq. (24).

$$k_2 = \frac{u_v - k_1 \dot{x}_p}{F_L} \tag{30}$$

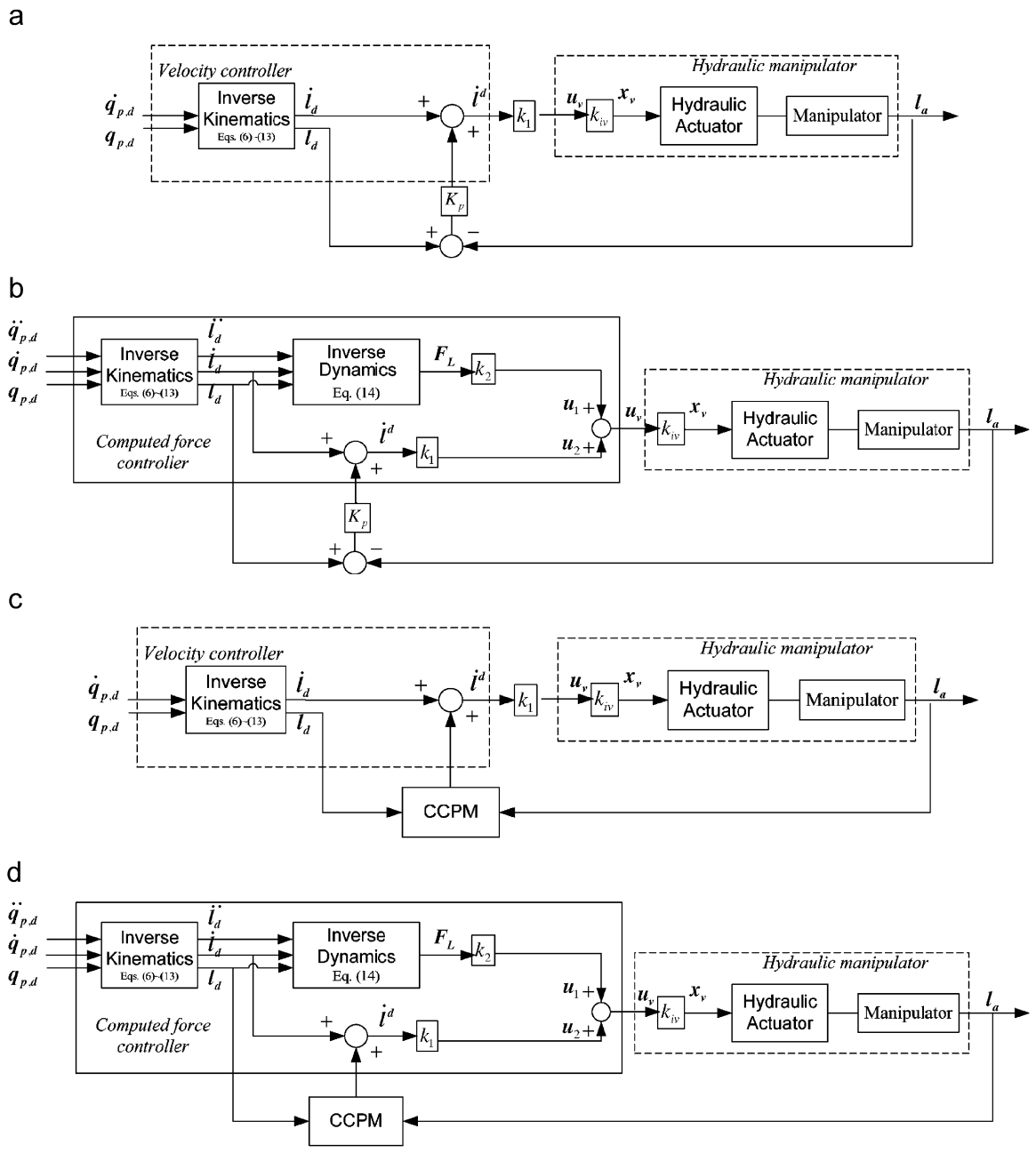

Fig. 9. (a) Velocity control for hydraulic parallel manipulator. (b) Velocity control with force computation for hydraulic parallel manipulator. (c) Velocity control with cross-coupled pre-compensation for hydraulic parallel manipulator. (d) Velocity control with cross-coupled pre-compensation and force computation for hydraulic parallel manipulator.

and

$$k_2^{cyl1} = 0.0470\left(\frac{\text{voltage}}{\text{Newton}}\right), \quad k_2^{cyl2} = 0.0314\left(\frac{\text{voltage}}{\text{Newton}}\right),$$
$$k_2^{cyl3} = 0.0314\left(\frac{\text{voltage}}{\text{Newton}}\right).$$

The average force F_L provided by each cylinder is about 100 N.

The inverse dynamics, see Fig. 9(b) and (d), is utilized to calculate the hydraulic actuating force. Basically, parameters can be obtained by identification (Guegan, Khalil, & Lemoine, 2003), but in this work the parameters are estimated by CAD software and the parameters are listed in Table 1. Besides, feedback gain K_p is empirically chosen 20 for good error convergence. No optimization of the controller gains (Kim & Lee, 2006) or feed back linearization (Seo, Venugopal, & Kenné, 2007) is pursued in this work.

5.3. Experimental results and discussion

Two trajectories as listed in Table 2 are used to evaluate the hydraulic parallel manipulator system. In the first series

of experiments, the effect of force computation is evaluated. Hydraulic parallel manipulator tracks both trajectories under pure velocity control with and without force computation. Fig. 12 shows the results. In the second series of experiments, the manipulator tracks both trajectories under two different controls: velocity control with cross-coupled pre-compensation (CCPM), velocity control with CCPM and force computation. Fig. 13 shows the results of the second series experiments.

All trajectory tracking were performed under 38.5 kg payload. And the error index, IAE (integral absolutely error), is given by

$$\mathrm{IAE} = \int_t |e(t)|\,\mathrm{d}t = \sum^{n} |e(t)|T_s \quad \text{(discrete-time)}. \tag{31}$$

Trajectory 1. $Z(t) = 600 + 10t, \quad \alpha(t) = 0, \quad \beta(t) = (\pi/18)\sin(0.4\pi t)$.

Trajectory 2. $Z(t) = 650 + 5t, \quad \alpha(t) = (\pi/16)\cos(1.2\pi t), \quad \beta(t) = (\pi/16)\sin(1.2\pi t)$.

Table 3 compares the error index IAE from Fig. 12. It is reasonable that for pure velocity control, IAE of tracking trajectory 2 enlarged as can be seen from Fig. 12(c) and (d) and Table 3. It is interesting that force computation reduces the error index remarkably. Table 3 reveals that for trajectory 1 the force computation reduces the IAE value of cylinders 3 to 52.7% but it appears no substantial improvement in cylinders 1 and 2. For trajectory 2 force computation improves IAE value of cylinder 1 and 2 but, again, there is no substantial improvement for cylinder 3.

Generally, trajectory 1 is slower tracking while trajectory 2 is faster tracking. It is seen from Table 3 that the effect of force computation is more apparent in the faster tracking.

Fig. 10. Hydraulic motion platform.

Table 1
Estimated physical parameters

Mass inertia (kg)		Moment inertia (kg m^2)	
Piston	6.5	$I_{\text{axis}}^{\text{upper}}$	5
Cylinder	7.3	$I_{\text{axis}}^{\text{lower}}$	7
Motion platform	8.5	$I_{\text{xx}}^{\text{platform}}$	0.4538
Dimension of platform		$I_{\text{yy}}^{\text{platform}}$	0.7938
$\varphi_a = \varphi_b$	800 mm	$I_{\text{zz}}^{\text{platform}}$	1.2467
θ	120°	Load carry (kg)	38.5

Table 2
Trajectories used in experiments

Trajectory 1	$Z(t) = 600 + 10t, \quad \alpha(t) = 0, \quad \beta(t) = (\pi/18)\sin(0.4\pi t)$
Trajectory 2	$Z(t) = 650 + 5t, \quad \alpha(t) = (\pi/16)\cos(1.2\pi t), \quad \beta(t) = (\pi/16)\sin(1.2\pi t)$

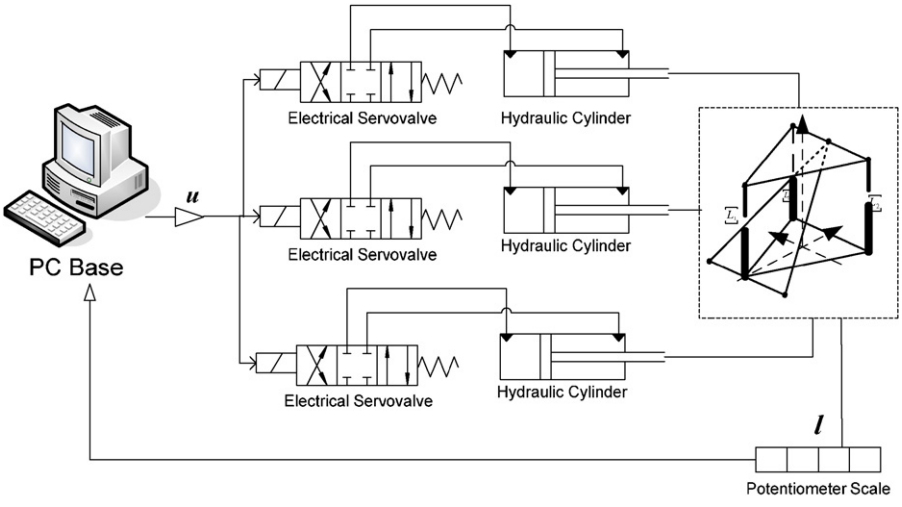

Fig. 11. Experimental hydraulic manipulator system.

Figs. 13(a) and (b) are results of velocity control with cross-coupling pre-compensation and velocity control with cross-coupling pre-compensation as well as force computation. These results evaluate the effect of cross-coupling contour tracking combined with force computation. Table 4 lists the quantified error index IAE values. In trajectory 1, while cylinder 1 obtained significant improvement, cylinders 2 and 3 have bigger IAE values. The IAE

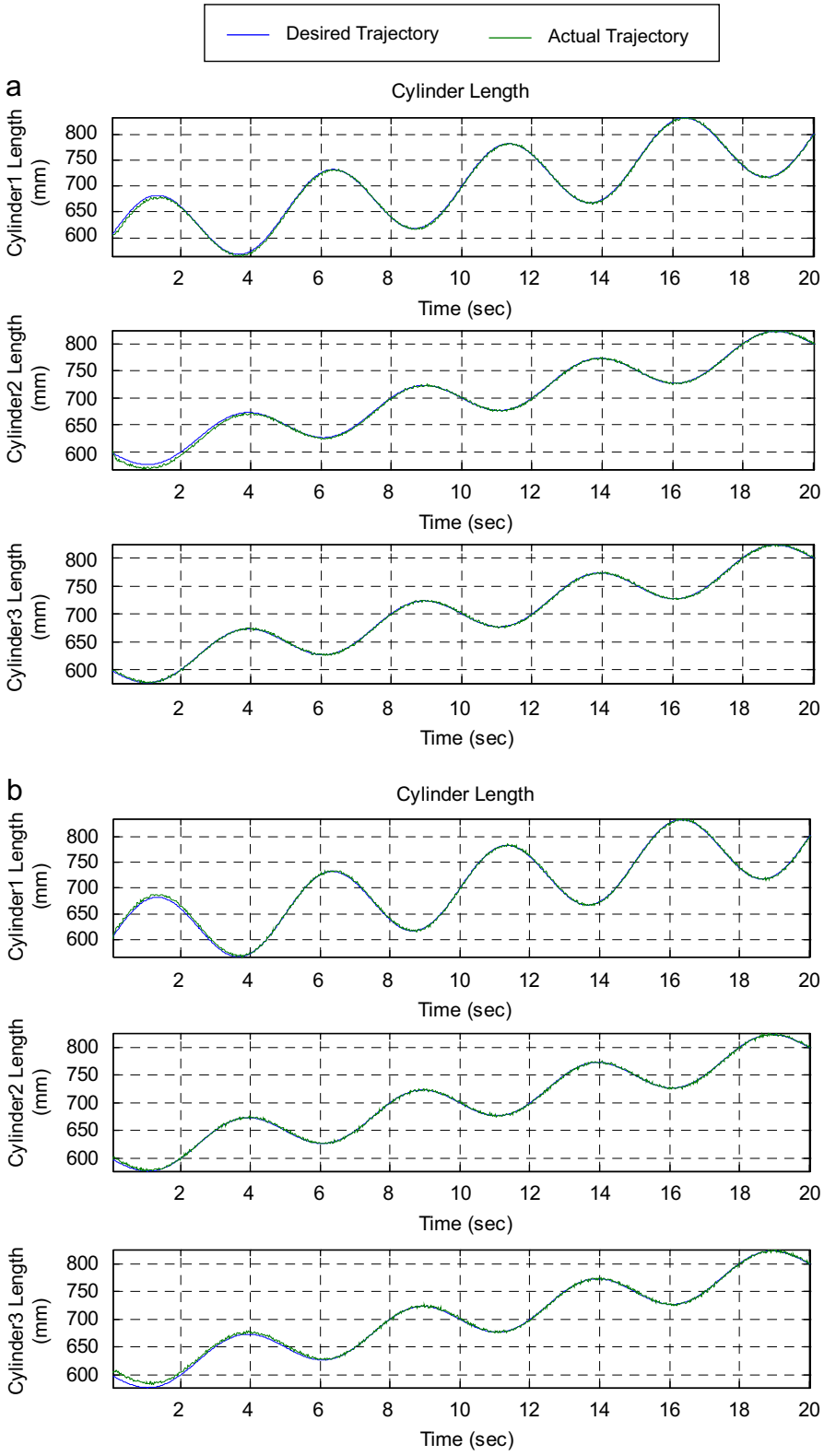

Fig. 12. Tracking under velocity control (a) *without* and (b) with computed force (trajectory 1). Cylinder tracking (c) *without* and (d) with computed force (trajectory 2).

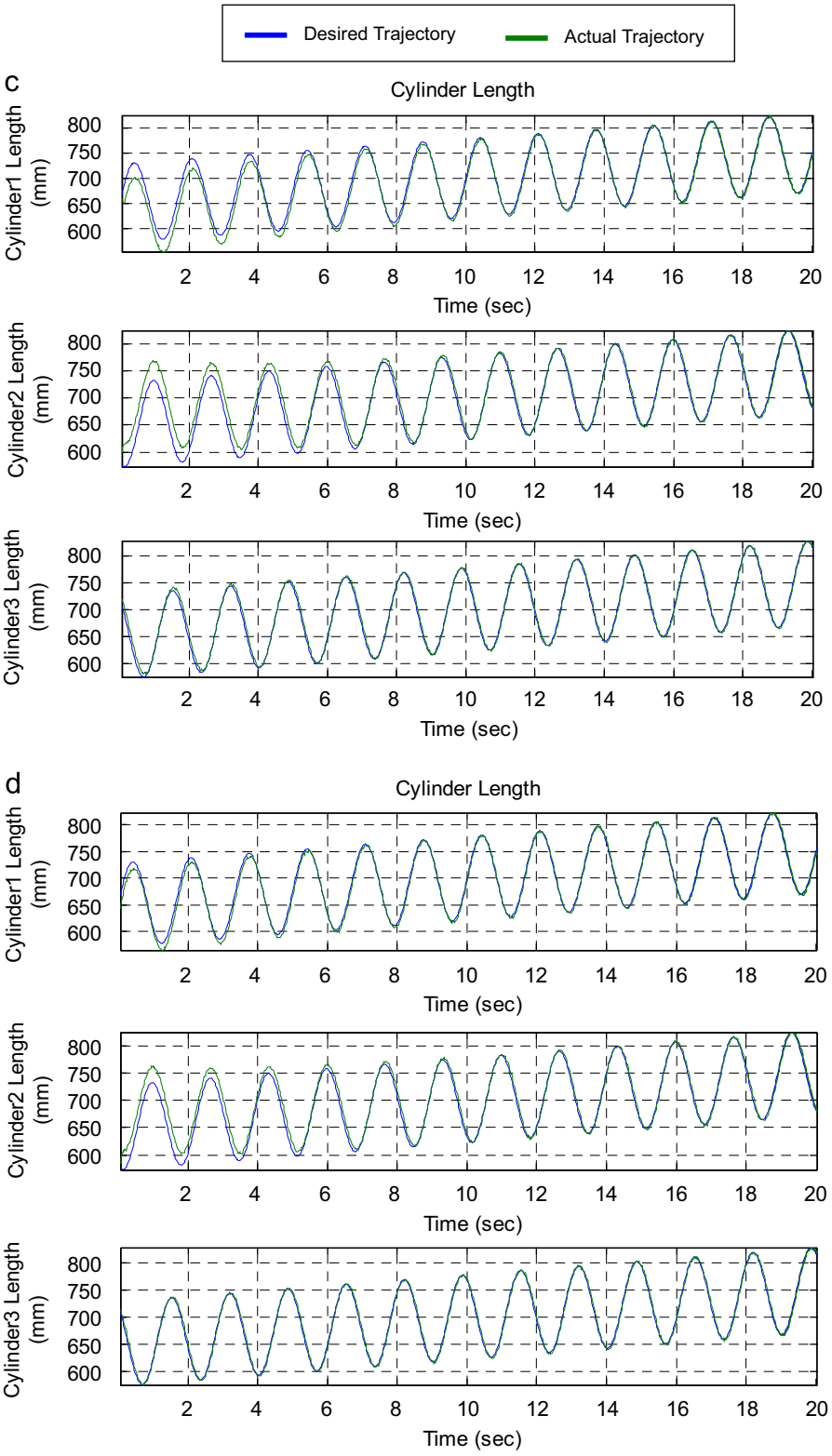

Fig. 12. (*Continued*)

value of cylinder 3 became 1.86 times. This may be caused by the trajectory type because in trajectory $\alpha = 0$ and the trajectory is not in a closed form. In trajectory 2, the IAE value of cylinders 2 and 3 has mild improvement but that of cylinder 3 is insignificant.

The slight dead-zone non-linearity characteristics in the relations between spool displacement and cylinder velocity do not seem to cause trouble. There is no need for specific measure to deal with the non-linearity of dead-zone.

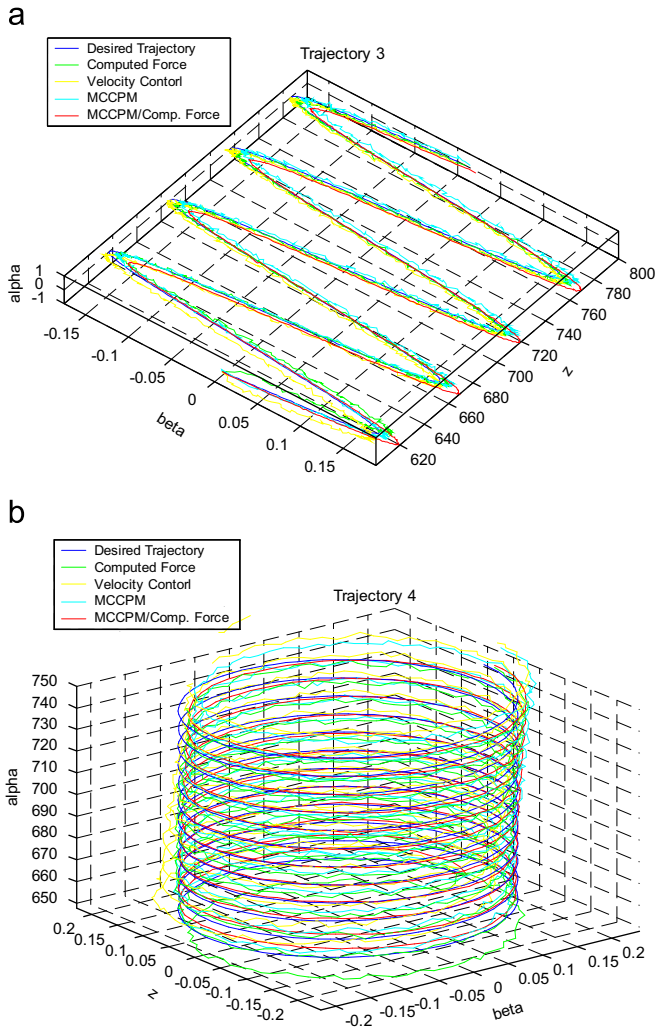

Fig. 13. (a) $Z(t) = 600 + 10t$, $\alpha(t) = 0$, $\beta(t) = (\pi/18)\sin(0.4\pi t)$ (trajectory 1). (b) $Z(t) = 650 + 5t$, $\alpha(t) = (\pi/16)\cos(1.2\pi t)$, $\beta(t) = (\pi/16)\sin(1.2\pi t)$ (trajectory 2).

Table 3
IAE results for trajectory tracking in Fig. 12 (Experiment 1)

Trajectory number	Controller type	Cylinder 1	Cylinder 2	Cylinder 3
1	Pure velocity control	41.0597	46.7235	47.2582
	With computed force	39.8707	43.7352	24.9348
2	Pure velocity control	162.8768	202.9674	88.6916
	With computed force	97.3378	176.5577	83.3361

Generally, it is seen that the force computation improves the link tracking precision for regular control like velocity control. Since contour tracking manipulates individual link to cross-compensate other links' errors, it often interferes into link behavior in order to improve precision in work space. Thus for contour tracking, force computation may conditionally improve the tracking precision, depending upon the trajectory type.

6. Conclusions

Machine tools have excellent continuous path tracking ability; however, the feeding control usually does not compute force. Robots have excellent spatial mobility with limited continuous path tracking ability, whereas their standard motion control includes force computation. Parallel manipulators are a family of machines resembling robots and have significant potential to become machine tools or a sub-system of machine tools. To transform parallel manipulators into machine tools, continuous path tracking, a contour tracking algorithm, and force computation are integrated. This work addresses the integration of continuous path tracking, a contour tracking algorithm and force computation on a hydraulic parallel manipulator.

An empirical hydraulic parallel manipulator is constructed and a control algorithm is proposed in this work. Based on the control algorithm, four control systems, velocity control, velocity control with force computation, velocity control with contour tracking, and velocity control with cross-coupling pre-compensation contour tracking and force computation are constructed and experimented.

The force computation reduced tracking error. The effect of force computation is especially true for high speed tracking. For contour tracking, the effect of force computation is also true; however, it may interfere with cross-coupling effects and neutralize improvements, or cause slight negative effects to one or two manipulator links.

This work has established continuous path tracking ability for hydraulic parallel manipulator using a control law that includes both force computation and tracking control. It is concluded that, although machine tools do not compute forces when creating feeding motion, the parallel, specifically a hydraulic parallel manipulator, should include force computation in the tracking algorithm, just like robots.

Table 4
IAE results for trajectory tracking in Fig. 13 (Experiment 2)

Trajectory number	Controller type	Cylinder 1	Cylinder 2	Cylinder 3
1	Velocity with MCCPM	43.2597	34.4584	24.5886
	Velocity with computed force and MCCPM	28.2688	36.7982	45.8500
2	Velocity with MCCPM	183.4489	181.3060	91.3014
	Velocity with computed force and MCCPM	74.4102	89.7602	81.6863

Acknowledgments

The authors thank the National Science Council of Republic of China for the financial support of this work under Grant no. NSC-93-2212-E-009-021.

Appendix A. Supplementary materials

Supplementary data associated with this article can be found in the online version at doi:10.1016/j.conengprac.2007.08.007

References

Benallegue, A. (1995). Adaptive control for flexible-joint robots using a passive systems approach. *Control Engineering Practice*, *3*(10), 1393–1400.

Cheng, Y.-M. (2004). *Precision trajectory tracking for multi-axis motion platform of serial and parallel structure*. Dissertation, National Chiao Tung University.

Cheng, Y.-M., & Chin, J.-H. (2003). Machining contour errors as ensembles of cutting, feeding and machine structure effects. *International Journal of Machine Tools and Manufacture*, *43*, 1001–1014.

Chin, J.-H., Cheng, Y.-M., & Lin, J.-H. (2004). Improving contour accuracy by fuzzy logic enhanced cross-coupled precompensation method. *Robotics and Computer Integrated Manufacturing*, *20*, 65–76.

Chin, J.-H., & Lin, T.-C. (1997). Cross-coupled precompensation method for the contouring accuracy of computer numerically controlled machine tools. *International Journal of Machine Tools and Manufacture*, *37*(7), 947–967.

Chin, J.-H., & Lin, H.-W. (1999). The algorithms of the cross-coupled precompensation method for generating the involute-type scrolls. *ASME Journal of Dynamic Systems, Measurement, and Control*, *121*(1), 96–104.

Chin, J.-H., Peng, X.-E. (2005a). A tracking simulation for a hybrid Stewart platform manipulator. In *Proceedings of the IASTED International Conference on Modelling and Simulation*, Cancun, Mexico.

Chin, J. H., & Tsai, H. C. (1993). A path algorithm for robotic machining. *Robotics and Computer-Integrated Manufacturing*, *10*(3), 185–198.

Dasgupta, B., & Mruthyunjaya, T. S. (1998a). Closed-form dynamic equations of the general Stewart platform through the Newton–Euler approach. *Mechanism and Machine Theory*, *33*(7), 993–1012.

Dasgupta, B., & Mruthyunjaya, T. S. (1998b). A Newton-Euler formulation for the inverse dynamics of the Stewart platform manipulator. *Mechanism and Machine Theory*, *33*(8), 1135–1152.

Dasgupta, B., & Mruthyunjaya, T. S. (2000). The Stewart platform manipulator: A review. *Mechanism and Machine Theory*, *35*(1), 15–40.

Gang, F. (1990). A new adaptive control algorithm for robot manipulators in task space. *IEEE Transactions on Robotics and Automation*, *11*(3), 457–462.

Geng, Z., Haynes, L. S., Lee, J. D., & Carroll, R. L. (1992). On the dynamic model and kinematics analysis of a class of Stewart platforms. *Robotics and Autonomous System*, *9*, 237–254.

Gosselin, C., & Angeles, J. (1989). The optimum kinematic design of a spherical three-degree-of-freedom parallel manipulator. *Journal of Mechanism, Transmissions and Automation in Design*, *111*(2), 202–207.

Gosselin, C., & Angeles, J. (1990). Kinematic inversion of parallel manipulators in the presence of incompletely specified tasks. *ASME Journal of Mechanical Design*, *112*(4), 494–500.

Guegan, S., Khalil, W., & Lemoine, P. (2003). Identification of the dynamic parameters of the orthoglide. In *IEEE International Conference on Robotics and Automation* (pp. 3272–3277).

Harib, K., & Srinivasan, K. (2003). Kinematic and dynamic analysis of Stewart platform-based machine tool structures. *Robotica*, *21*, 541–554.

Honegger, M. (1997). Adaptive control of the Hexaglide, a 6 DOF parallel manipulator. In *Proceedings of IEEE ICRA*, Albuquerque NM, USA.

Huan, J. (1982). *Trajectory regulation for creation of trajectory on numerically controlled machine tools*. Dissertation, University of Stuttgart (in German).

Ibrahim, O., Khalil, W., & Guegan, S. (2004). Dynamic modelling of some parallel robots. In *ISR International Symposium on Robotics*, Paris, France.

Khalil, W., Gallot, G., & Boyer, F. (2005). Dynamic Modeling and Simulation of a 3-D Serial Eel-Like Robot. *IEEE International Conference on Robotics and Automation*, 1270–1275.

Khalil, W., & Guegan, S. (2004). Inverse and Direct Dynamic Modeling of Gough-Stewart Robots. *IEEE Transactions on Robotics and Automation*, *20*(4), 754–762.

Kim, M. Y., & Lee, C-O. (2006). An experimental study on the optimization of controller gains for an electro-hydraulic servo system using evolution strategies. *Control Engineering Practice*, *14*(2), 137–147.

Koren, Y. (1980). Cross-coupled biaxial computer control for manufacturing systems. *ASME Trans Journal of Dynamic System, Measurement and Control*, *102*(4), 265–272.

Koren, Y., & Lo, Ch.-Ch. (1991). Variable gain cross coupling control for contouring. *Annals of the CIRP*, *40*, 371–374.

Kosuge, K., Takeo, K., Fukuda, T., Kitayama, H., Takeuchi, N., & Murakami, H. (1996). Force control of parallel link manipulator with hydraulic actuators. *International Conference on Robotics and Automation*, 305–310.

Kwon, D.S., Babcock, S.M. (1995). Tracking control on the hydraulically actuated flexible manipulator. In *IEEE International Conference on Robotics and Automation*, 3, 2200–2205.

Lischinsky, P., Canudas-de-Wit, C., & Morel, G. (1999). Friction compensation for an industrial hydraulic robot. *Control Systems Magazine, IEEE*, *19*(1), 25–32.

Liu, G. P., & Daley, S. (2000). Optimal-tuning nonlinear PID control of hydraulic systems. *Control Engineering Practice*, *8*(9), 1045–1053.

Lue, C.-W., Cheng, Y.-M., & Chin, J.-H. (2005). System structure and contour tracking for a hybrid motion platform. *International Journal of Advanced Manufacturing Technology*, *26*, 1388–1396.

Merlet, J.-P. (1992). Direct kinematics and assembly modes of parallel manipulators. *International Journal of Robotics Research*, *11*(2), 150–162.

Merlet, J.-P. (2000). *Parallel robots. INRIA Sophia-Antipolis, solid mechanics and its Applications*, Vol. 74. Dordrecht: Kluwer Academic Publishers.

Merlet, J.-P., Perng, M.-W., & Daney, D. (2000). Optimal trajectory planning of a 5-axis machine tool based on a 6-axis parallel manipulator. *ARK, Piran*, *25*(2), 315–320.

Merrit, H. E. (1967). *Hydraulic control systems*. New York: Wiley.

Raghavan, M. (1993). Stewart platform of general geometry has 40 configurations. *Transaction ASME, Journal of Mechanical Design*, *115*(2), 277–280.

Rolf, J. (1990). Adaptive control of robot manipulator motion. *IEEE Transaction on robotics and automation.*, *6*(4), 483–490.

Sarachik, P., & Ragazzini, J. R. (1957). A two dimensional feedback control system. *Transaction AIEE*, *76*, 55–61.

Sekhavat, P., Sepehri, N., & Wu, Q. (2006). Impact stabilizing controller for hydraulic actuators with friction: Theory and experiments. *Control Engineering Practice*, *14*(12), 1423–1433.

Seo, J., Venugopal, R., & Kenné, J.-P. (2007). Feedback linearization based control of a rotational hydraulic drive. *Control Engineering Practice*. doi:10.1016/j.conengprac.2007.02.009

Siciliano, B., & Villani, L. (1996). Adaptive compliant control of robot manipulators. *Control Engineering Practice*, *4*(5), 705–712.

Sirouspour, M. R., & Salcudean, S. E. (2001). Nonlinear control of a hydraulic parallel manipulator. *IEEE Transaction Robotics and Automation*, *17*(2), 173–182.

St-Onge, B. M., & Gosselin, C. M. (2000). Singularity analysis and representation of the general Gough–Stewart platform. *International Journal of Robotics Research*, *1*(3), 271–288.

Tsai, L.-W. (1996). Kinematics of a three-DOF platform with three extensible limbs. In J. Lenarcic, & V. Parenti-Castelli (Eds.), *Recent advances in robot kinematics* (pp. 401–410). Dordrecht: Kluwer Academic Publishers.

Tsai, L.-W. (1999). *Robot analysis—The mechanics of serial and parallel manipulators*. New York: Wiley.

Tsai, L.-W. (2000). Solving the inverse dynamics of a Stewart-Gough manipulator by the principle of virtual work. *ASME Journal of Mechanical Design*, *122*, 3–9.

Tsai, L.-W., & Joshi, S. A. (2003). The kinematics of a class of 3-DOF, 4 legged parallel manipulators. *ASME Journal of Mechanical Design*, *125*, 52–60.

Walker, M.W., Wee, L.-B. (1991). An adaptive control strategy for space based robot manipulators. In *Proceedings of the IEEE ICRA, Sacramento CA, USA*.

〈www.parallemic.org〉.

Zhou, J. (1995). Experimental evaluations of a kinematic compensation control method for hydraulic robot manipulators. *Control Engineering Practice*, *3*(5), 675–684.